
This is an electronic reprint of the original article.
This reprint may differ from the original in pagination and typographic detail.

Mikkonen, Marko; Laakso, Ilkka; Tanaka, Satoshi; Hirata, Akimasa

Cost of focality in TDCS

Published in:
Brain Stimulation

DOI:
[10.1016/j.brs.2019.09.017](https://doi.org/10.1016/j.brs.2019.09.017)

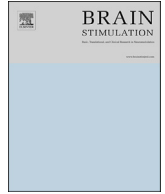
Published: 01/01/2020

Document Version
Publisher's PDF, also known as Version of record

Published under the following license:
CC BY

Please cite the original version:
Mikkonen, M., Laakso, I., Tanaka, S., & Hirata, A. (2020). Cost of focality in TDCS: Interindividual variability in electric fields. *Brain Stimulation*, 13(1), 117-124. <https://doi.org/10.1016/j.brs.2019.09.017>

This material is protected by copyright and other intellectual property rights, and duplication or sale of all or part of any of the repository collections is not permitted, except that material may be duplicated by you for your research use or educational purposes in electronic or print form. You must obtain permission for any other use. Electronic or print copies may not be offered, whether for sale or otherwise to anyone who is not an authorised user.



Cost of focality in TDCS: Interindividual variability in electric fields

Marko Mikkonen^{a,*}, Ilkka Laakso^a, Satoshi Tanaka^b, Akimasa Hirata^c

^a Aalto University, Department of Electrical Engineering and Automation, Finland

^b Hamamatsu University School of Medicine, Japan

^c Nagoya Institute of Technology, Department of Electrical and Mechanical Engineering, Japan

ARTICLE INFO

Article history:

Received 23 April 2019

Received in revised form

25 September 2019

Accepted 29 September 2019

Available online 2 October 2019

Keywords:

TDCS

Focality

HD-TDCS

Interindividual variability

Electric field

ABSTRACT

Background: In transcranial direct current stimulation (TDCS), electric current is applied via two large electrodes to modulate brain activity. Computational models have shown that large electrodes produce diffuse electric fields (EFs) in the brain, which depends on individual head and brain anatomy. Recently, smaller electrodes as well as novel electrode arrangements, including high-definition TDCS (HD-TDCS) montages, have been introduced to improve the focality of EFs. Here, we investigated whether the EFs of focal montages are more susceptible to interindividual anatomical differences.

Methods: Thirteen TDCS montages, including conventional M1-contralateral forehead montages with different stimulating electrode sizes as well as 4×1 HD and bipolar HD montages, producing varying EF focalities were modeled using the finite element method in 77 subjects, with individual anatomically realistic models based on magnetic resonance images.

Results: Interindividual variability of predicted EFs increased with EF focality for conventional M1-contralateral forehead and 4×1 HD montages. 4×1 HD-TDCS was found to have the highest EF focality and greatest variability. Bipolar HD montages targeting the region between two small electrodes did not follow this pattern, but produced EF magnitudes comparable to those of 4×1 HD-TDCS, with a minor decrease in focality and lower interindividual variability.

Conclusions: EF focality in TDCS was achieved at the cost of increased interindividual variability. Hence, individual modeling is required to plan EF doses when focal montages are used. Among the studied montages, bipolar HD montages provided a compromise between inter-individual variability, focality and magnitude of the predicted EFs.

© 2019 The Author(s). Published by Elsevier Inc. This is an open access article under the CC BY license (<http://creativecommons.org/licenses/by/4.0/>).

Introduction

In recent decades, noninvasive brain stimulation has become widely used for studying and treating various neurological and psychiatric disorders. Methods such as transcranial direct current (TDCS) and magnetic (TMS) stimulation are capable of modulating brain activity beyond the duration of stimulation and have potential in the treatment of diseases including depression [1], chronic pain [2] and motor and sensory deficits after stroke [3–5].

Conventionally, 1–2 mA electric currents are applied in TDCS via two 25–35 cm² electrodes [6], producing spatially widespread electric fields (EFs) on the cerebral cortex [7,8]. Although promising results have been obtained using these montages, results vary between subjects [9,10]. Computational models suggest that this variability may be partially due to differences in individual anatomy

[11,12]. As recent studies have also pointed out the importance of both EF magnitude and direction [13–16] on the cerebral cortex to the stimulation outcome, better control of stimulation is required.

Improved stimulation control has been attempted by better targeting of EFs. Previous studies have used various approaches to achieve more localized EF distribution: smaller stimulating electrodes have been found to produce more focal TDCS [17–20], and various high-definition [8,21] and multifocal [22] TDCS setups have been developed. These are often used with the same input currents (1–2 mA) as traditional montages, although montage selection affects EFs. As individual anatomy also affects TDCS EFs, increasing the focality of stimulation could result in greater uncertainty in group-level results due to EFs being more affected by local individual anatomy.

Here, we computationally examined TDCS EFs in 77 subjects using 13 different TDCS montages to produce different EF focalities. The objective was to determine how the montage affects the interindividual variability in TDCS EFs in the hand area of the primary motor cortex (M1).

* Corresponding author., Rakentajanaukio 2, 02150, Espoo, Finland.
E-mail address: marko.mikkonen@aalto.fi (M. Mikkonen).

Methods

Subjects

We used T1- and T2-weighted magnetic resonance (MR) images obtained with 3 T scanners from 77 neurologically healthy subjects (58 males) in our prior studies [7,13,23,24]. All subjects provided informed and written consent prior to participating in MR imaging (MRI). Subjects had an average age of 25 years, ranging from 19 to 47 years.

Segmentation

The obtained T1- and T2-weighted MR images were used to build volume conductor models with a resolution of $0.5 \times 0.5 \times 0.5 \text{ mm}^3$ using both FreeSurfer [25–28] and a previously described in-house method [11,24]. FreeSurfer was used to segment the brain into gray and white matter. Tessellated surfaces of gray and white matter were also generated using FreeSurfer. Brain segmentation was improved by segmentation of subcortical structures (nuclei, cerebellum, and brainstem) and ventricles. Non-brain tissues were segmented by first dividing them into three compartments consisting of the scalp, skull, and the space between the skull and the brain (intracranial compartment). The compartments were finally segmented based on both the T1- and T2-weighted images and morphological information into the following tissues: scalp into skin, muscle, and fat; skull into compact and cancellous bone; and intracranial compartment into cerebrospinal fluid (CSF), venous sinuses (blood), and dura. The continuity of the CSF layer was ensured during the segmentation process.

Electrical conductivities

To generate volume conductor models, electrical conductivity was assigned to each voxel in the segmented head models. Conductivities were assumed to be linear and isotropic. For gray matter, we used 0.2 S/m, based on the average of previously reported values [29–34], and for white matter, 0.14 S/m, which is 30% lower than the gray matter values, in accord with previously reported values [29–31]. These conductivities were also used for cerebellar gray and white matter. CSF conductivity was 1.8 S/m [35]. Other conductivity values were: blood, 0.7 S/m [31]; compact and cancellous bone, 8 mS/m and 27 mS/m, respectively [36] (bone conductivities were increased by 30% to compensate for room temperature measurement. The factor of the increase was estimated based on tissue conductivity measurements at room and body temperatures [30]); muscle and dura were assumed to have the same conductivity, 0.16 S/m [37]; skin, 0.08 S/m [37]; fat, 0.08 S/m [37]; and eye tissue, 1.5 S/m [38].

Computational model and solution methods

The EF (V/m) can be represented as

$$E = -\nabla\phi, \quad (1)$$

where the electric scalar potential ϕ (V) satisfies the following equation and boundary conditions

$$\begin{cases} \nabla \cdot \sigma \nabla \phi = i, & \text{in } \Omega \\ \frac{\partial \phi}{\partial n} = 0, & \text{on } \partial\Omega, \end{cases} \quad (2)$$

where domain Ω contains both the head and the electrodes, $\partial\Omega$ is the boundary of Ω , σ denotes the electrical conductivity (S/m), and i

is the applied current source/sink density (A/m^3). The applied source/sink density i is nonzero only at the electrodes and satisfies equations $\int i dV = 0$ and $\frac{1}{2} \int |i| dV = I$, where the integrals are taken over Ω and I (A) is the input current. The electrode models and montages are described in detail in the next section.

To numerically determine ϕ , equation (2) was discretized using the finite element method (FEM), using voxels of the volume conductor model as elements. Likewise, the electrodes were modeled using cubical elements. The basis functions were linear. On average, the models, including the electrodes, consisted of 33 million cubical elements sized $0.5 \times 0.5 \times 0.5 \text{ mm}^3$, with 34 million degrees of freedom. The linear equation system resulting from discretization was solved using the geometric multigrid method [39].

After ϕ was determined, EFs were calculated at the vertices ($N \approx 142000$) of a tessellated surface located 1 mm below the gray matter surface from (1).

Additionally, EFs induced by TMS were determined using the same solver for scalar potential computations, but with a different source term. The details of the TMS computations and electric conductivities used here have been thoroughly described previously [7,23,40].

Electrode montages

We targeted stimulation to the right primary motor cortex. In Montreal Neurological Institute (MNI) coordinates, the target point was (42, −13, 66), which we have previously found to present the strongest correlation between the EF and motor evoked potentials in the left abductor pollicis brevis (APB) muscle [13]. The target point was projected from a template brain based on the MNI ICBM 2009a nonlinear asymmetric template [41,42] onto the cortex of each individual subject using FreeSurfer. The stimulating electrode (anode) was then centered onto the point closest to the target on the subject's scalp. The reference electrode (cathode) was placed on the contralateral forehead (Fp1 of the EEG 10/20 system), as is often done when stimulating the motor cortex [6]. Here, “electrode” refers to the combination of a saline-soaked sponge, rubber pad enclosed within the sponge, and a connector enclosed in rubber to which the electric current is applied. The electrode size and shape refer to those of the saline-soaked sponge.

The focality of TDCS improves as the size of the stimulating electrode diminishes [17–20]. Hence, we studied eight different stimulating electrode sizes and shapes. The three largest electrodes were quadrilateral: a large $10 \times 10 \text{ cm}^2$ square, which is sometimes used as the reference electrode [17], and the more common sizes of $7 \times 5 \text{ cm}^2$ and $5 \times 5 \text{ cm}^2$ [6]. Five round electrodes with diameters of 5, 4, 3, 2, and 1 cm were used to study the effects of smaller electrodes. Additionally, six round and square electrodes with surface areas of 0.79, 3.14, 7.07, 12.57, 19.63 and 28.27 cm^2 were used to study the effects of electrode shape on cortical EFs. For all of these cases, the size of the reference electrode was $5 \times 7 \text{ cm}^2$.

Because most focal EFs are achieved using high definition TDCS (HD-TDCS) montages, we studied a 4×1 concentric ring montage [8], in which a small stimulating electrode is surrounded by a ring of four small reference electrodes. In a previous study [43], the EFs produced by this kind of a montage have been found to become stronger and more diffuse with increasing distance between the stimulating and the reference electrodes. Hence, we considered three 4×1 HD montages with the four reference electrodes equally distributed around the stimulating electrode on a circle with radii of 3, 5 and 7 cm; labeled HD3, HD5 and HD7, respectively. Each electrode in the 4×1 HD montages had a diameter of 1.2 cm [44].

In addition, we studied two bipolar HD montages [14,16,45], in which two small (2 cm in diameter) round electrodes were placed 7 cm apart, with the target in the middle. The montages were

aligned 45° right and left from the anteroposterior direction and labeled ML and PA, respectively, following the nomenclature of [14].

All electrodes were modeled using a realistic design with two compartments and the shapes described earlier. Each electrode consisted of a 6-mm-thick saline soaked sponge with an electric conductivity of 1.6 S/m. The sponge encloses a 1-mm-thick rubber sheet (2/3 of the sponge diameter, $\sigma = 0.1$ S/m). The applied anodal/cathodal current was modeled by a current source/sink density distributed uniformly within a connector disk (radius 5 mm for each electrode size), located at the center of the rubber sheet. The input current was 1 mA in each case.

Finally, TMS was modeled as a comparative method. The TMS coil was modeled based on a Magstim 70-mm figure-8 coil using two circular coils with nine windings ranging from 7.2 cm to 9.7 cm in diameter [46]. The coil was placed in the same location as the stimulating electrode and oriented 45° from the anteroposterior direction.

Fig. 1 shows the electrode structure common to all TDCS montages used in this study, and Fig. 2 shows all of the individual electrode montages and the TMS setup.

To generalize the findings, the calculations were repeated for three additional targets (F4, C6 and O2 of the EEG 10/20 system). Conventional montages with stimulating electrodes sized 5×7 cm² and $\emptyset 2$ cm and extracephalic reference electrodes, and HD5 and PA montages were studied.

Data analysis

For group-level analysis, the individual EF magnitudes and normal components calculated on the vertices on a tessellated surface 1 mm below the surface of the gray matter were registered to a common template brain surface, generated using FreeSurfer from the MNI template brain.

To describe the overall strength and distribution of the EFs, the median (over all 77 subjects) magnitudes and normal components were determined at each vertex of the surface of right hemisphere of the template brain (149319 vertices). At each vertex, the inter-individual variability of the EF magnitude was measured in terms of the quartile coefficient of dispersion (QCD):

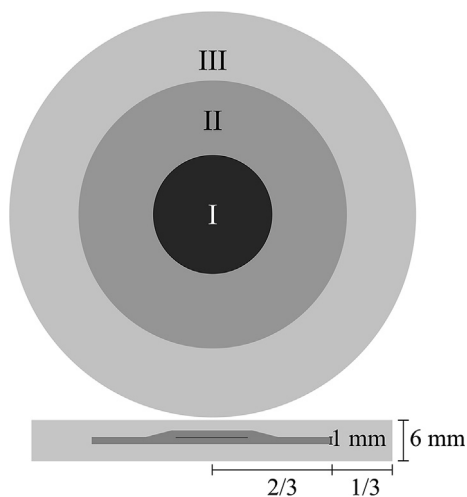


Fig. 1. Schematic of the electrodes used in this study. All electrodes were structured similarly: a 6-mm thick sponge (III) envelops a 1-mm thick rubber sheet (II), 2/3 of the size of the sponge, which further contained a $\emptyset 1$ cm connector disk (I) with uniformly distributed sources/sinks. The current was always 1 mA.

$$QCD = 100\% \times \left(\frac{Q_3 - Q_1}{Q_3 + Q_1} \right) \quad (3)$$

where Q_1 is the first and Q_3 the third quartile calculated over all 77 subjects.

The focality of the EF was calculated individually for each subject as the proportion of the surface area of the right hemisphere where the EFs exceeded 50% of the EF magnitude/normal component at the target point (hereafter referred to as $A_{1/2}$). To illustrate group-level $A_{1/2}$ and its variability for each electrode montage, the median values and QCD were calculated over all subjects.

To study the effects of anatomical features on the predicted EFs, the thicknesses of the skin, skull and CSF-layer beneath the center of the stimulating electrode were determined by finding the closest points to its center on the outer and inner skull surfaces, and on the cortex. Spearman's rank correlation coefficient was used to study the correlation between EF magnitude at the target point and the distances.

Results

Effects of electrode montage on EFs

EFs were calculated for all 13 TDCS montages and TMS in each of the 77 individual models at a tessellated surface 1 mm below the surface of the cortex and registered to the tessellated surface of the MNI template brain. This enabled us to calculate the across-subject median EFs and the QCD of EF magnitude in the whole right hemisphere. These values are presented in Fig. 2. We found a clear increase in the magnitude and focality of the EFs in the right hemisphere as the size of stimulating electrode diminished. The QCD exhibited the opposite pattern: the smaller the stimulating electrode, the higher the dispersion. The bipolar HD montages, ML and PA, also did not comply with this pattern: the EF magnitude at the target was comparable with that of the 4×1 HD montages, with variability in the range of that for TMS. The highest inter-individual variabilities in the EF magnitudes at the target point were obtained with the 4×1 HD montages, which also visually produced the most focal median EFs, as expected. However, the median EF magnitude at the target was higher with a $\emptyset 1$ cm stimulating electrode and PA montage than with the 4×1 HD montages.

Fig. 3A and B shows the EF magnitude at the target point and $A_{1/2}$ for each electrode montage, alongside their QCDs and interquartile (IQ) ranges. Heat maps in Fig. 3C and D shows the inter-montage differences in percentage points to better quantify how the changes in focality affect the inter-individual variability of EFs. The conventional montages with small stimulating electrodes produced higher median EF strengths and were more focal in the right hemisphere, in terms of having a smaller median $A_{1/2}$, compared with conventional montages with large stimulating electrodes: the difference between median $A_{1/2}$ of stimulating electrodes sized 10×10 cm² and $\emptyset 1$ cm was 64% points, with the $\emptyset 1$ cm stimulating electrode having a median $A_{1/2}$ of 5.9%. In addition, the QCD of the EF magnitude at the target was 6.7% points lower, with a stimulating electrode size of 10×10 cm² compared with a size of $\emptyset 1$ cm. However, with conventional montages, the variability of $A_{1/2}$ also increased towards more focal EFs with a five-fold increase in QCD of $A_{1/2}$ from stimulating electrodes sized 10×10 cm² to size $\emptyset 1$ cm. The 4×1 HD montages had the most focal EFs in the right hemisphere, with median $A_{1/2}$ ranging from 1.5% to 4.5%.

Additionally, the QCD of $|E|$ at the target and the median $A_{1/2}$ were found to have a strong negative correlation ($\rho = -0.95$), indicating that, as the focality of the EFs increased, the inter-individual

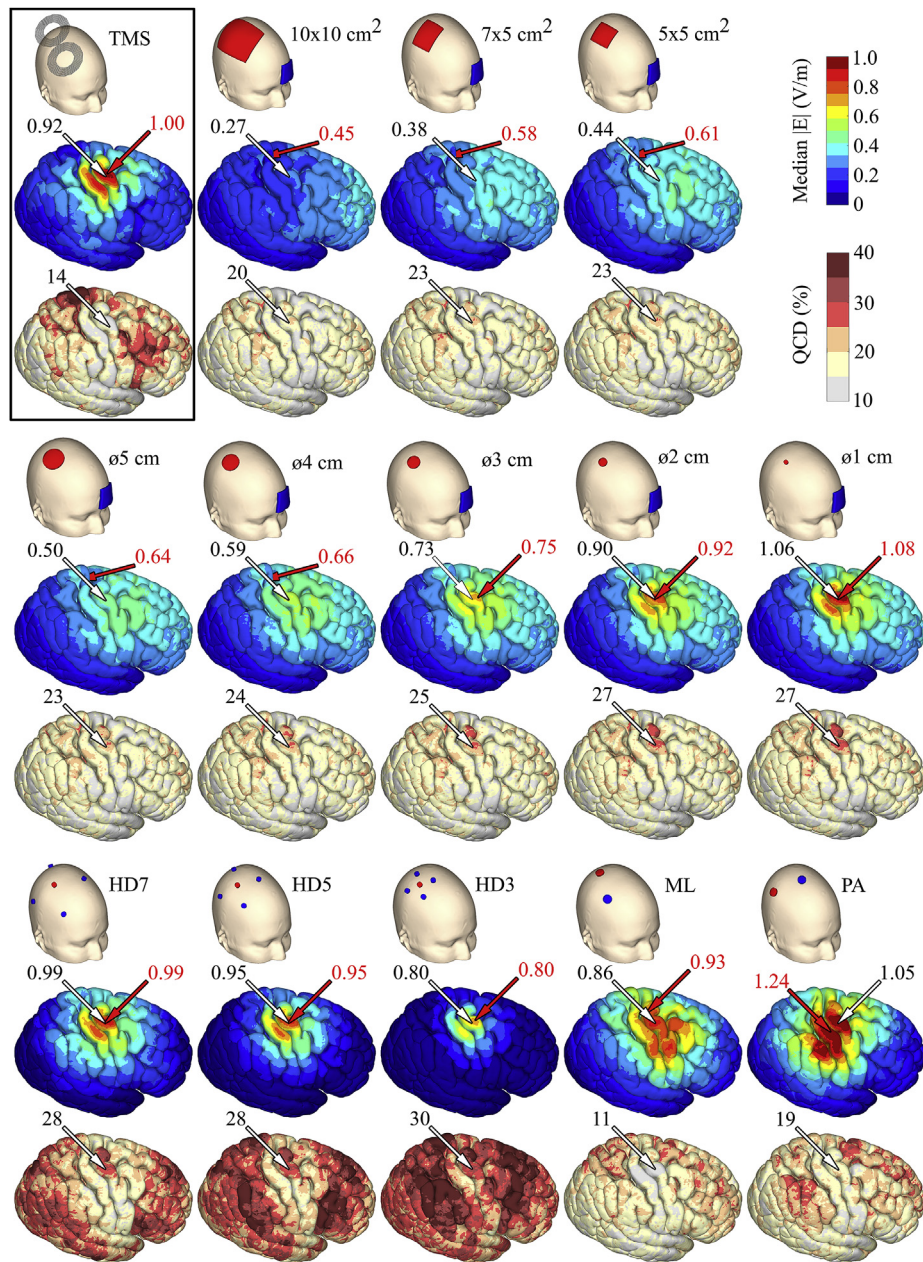


Fig. 2. Electrode montages, median EF magnitudes “Median $|E|$ ” and quartile coefficients of dispersion, QCD, of the EF magnitude presented on the template brain. Both “Median $|E|$ ” and QCD were calculated across the subjects at each vertex of the tessellated right hemisphere of the MNI template brain. White arrows indicate the target and show its Median $|E|$ and QCD, and red arrows indicate the location and magnitude of the maximum (over the vertices) “Median $|E|$ ”. The median TMS EFs are normalized so that the maximum median value equals one. The arrows presenting maximum values in the five conventional montages with the largest stimulating electrode sizes point to a hotspot at the bottom of the sulcus. (For interpretation of the references to colour in this figure legend, the reader is referred to the Web version of this article.)

variability of the EFs at the target also increased. The ML, PA and TMS montages were not included in the correlation analysis due to the differing montage types and visibly different patterns of results in Fig. 3A and B.

The data for the normal components is shown in Supplementary figures S1 and S2. In general, normal components behaved in a similar manner to the magnitude, with more focal montages producing higher and more variable normal components. However, the normal components of the ML, PA montages and TMS were smaller than for the other montages, although the magnitudes were at a similar level, which follows from a difference in the EF direction compared with the other TDCS montages.

Supplementary figure S3 presents data comparing square and round electrodes of six different sizes, and shows that the differences in the EFs are small between the two electrode shapes with the same surface area. Supplementary figure S4 shows data for three non-motor cortical stimulating/reference electrode locations. Although the exact magnitude, interindividual variability and focality differed between stimulating electrode locations for each montage, our general findings of conventional and 4×1 HD montages having higher interindividual variability with more focal EFs and bipolar HD montages producing different patterns of results appear to be valid, regardless of the location of the stimulating electrode.

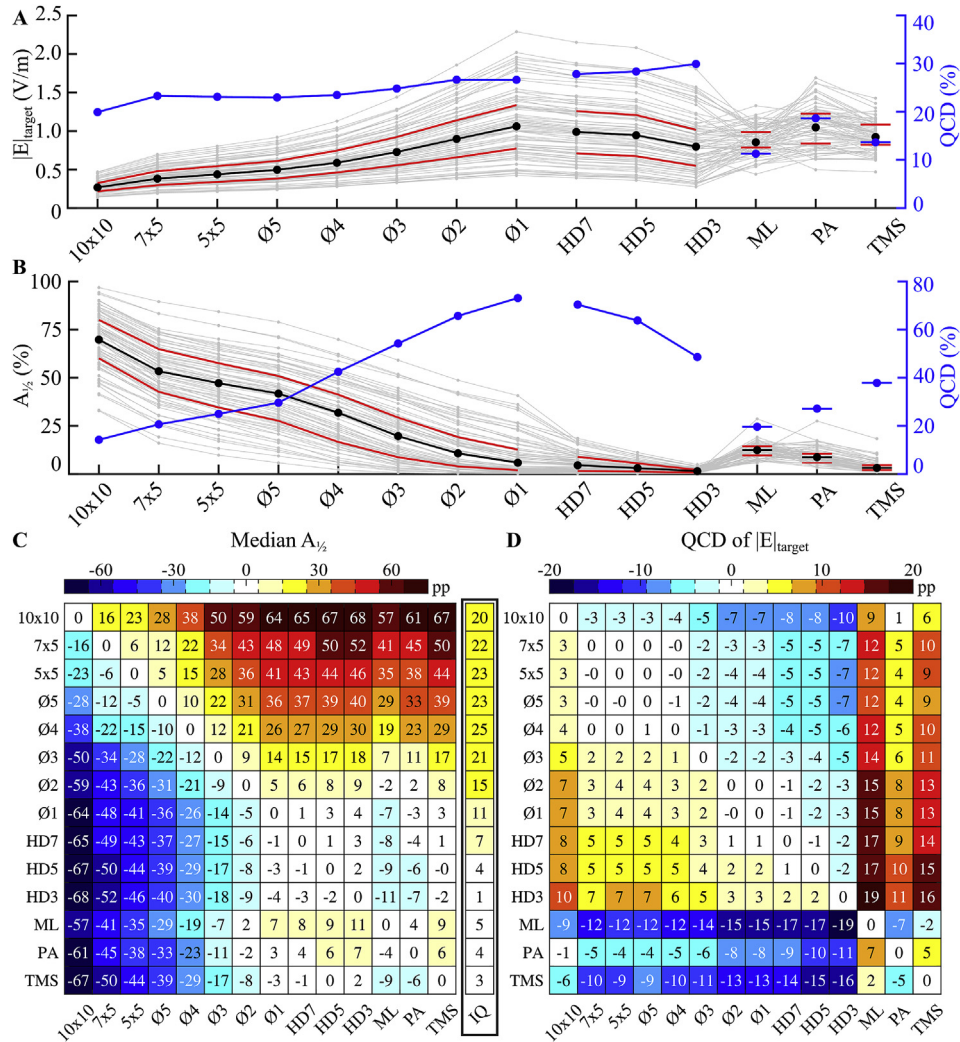


Fig. 3. Individual A) EF magnitude at the target point and B) $A_{1/2}$ for each montage (gray) and their corresponding medians (black). The red curves show the IQ range, and the blue curve shows the QCD. The TMS EFs are normalized so that the nodal maximum median value on the right hemisphere equals one. Heat maps C) and D) show the inter-montage differences (percentage points, pp) for median $A_{1/2}$ and QCD of $|E|_{\text{target}}$, respectively. The additional column in C) shows the IQ range for the focality of each montage to give an overview of the interindividual variability of the $A_{1/2}$ for each montage. (For interpretation of the references to colour in this figure legend, the reader is referred to the Web version of this article.)

Anatomical effects on EFs

As EFs are affected by the individual anatomy of the head, we studied whether the increase in the inter-individual variability in the predicted EFs due to increasing focality could be explained by changes in this effect. Fig. 4 shows the Spearman's rank correlation coefficient (ρ) for each electrode montage, representing the correlations between the EF magnitude at the target and the thicknesses of the scalp, skull, and CSF. On average, the thicknesses (mean \pm SD) were: scalp: 7.0 ± 1.0 mm, skull: 6.4 ± 1.3 mm, and CSF: 2.4 ± 1.2 mm. The thickness of the skull includes the thicknesses of the upper and lower compact layers (1.5 ± 0.3 mm and 1.5 ± 0.3 mm, respectively) as well as that of the spongiform layer (3.4 ± 1.2 mm).

As shown in Fig. 4, all correlations were negative, and the absolute value of the correlations increased as the stimulating electrode size decreased, suggesting that there was a minor connection between electrode size and the effect of individual anatomy. For bipolar HD montages, ρ was greatly affected by the orientation of the montage: the PA orientation showed larger effects of scalp

and skull thicknesses and smaller effect of CSF than the ML orientation.

Discussion

We examined the effects of different electrode montages on interindividual variability in TDCS using 77 subjects and 13 TDCS montages. We found that the interindividual variability of the predicted EFs increased systematically towards more focal EFs when using the conventional M1-contralateral forehead TDCS montage and the 4×1 HD-TDCS, which was found to produce both the most focal and the most variable EFs between individuals. Bipolar HD montages were found to provide the best compromise between EF variability, magnitude and focality.

In accord with previous reports [17–20], the current findings revealed an increase in the focality of EFs with decreasing stimulating electrode size. More focal EFs were also stronger at the target point. The most focal EFs, comparable with the focality of TMS, were found using a 4×1 HD-TDCS montage with a distance of 3 cm from the anode to the cathodes. The magnitude and focality of 4×1

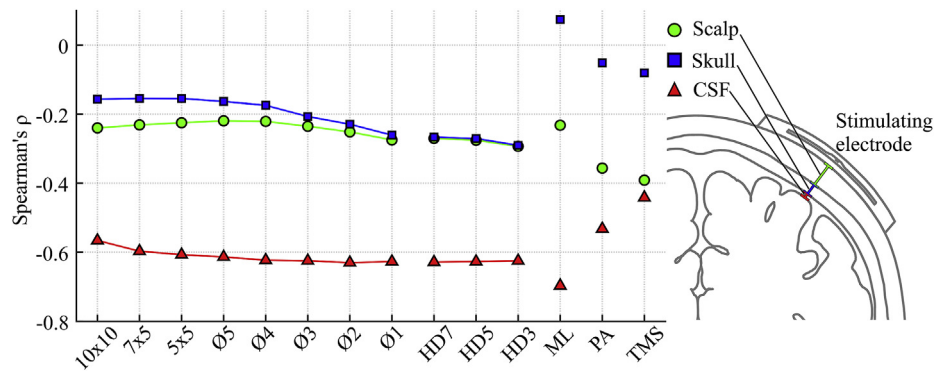


Fig. 4. Spearman's rank correlation coefficient (ρ) between the EF magnitude at the target and thickness of scalp (green), skull (blue) and CSF (red) for each montage. To calculate the distances, the closest points to the center of the stimulating electrode on the outer and inner skull surfaces and on the cortex were used. (For interpretation of the references to colour in this figure legend, the reader is referred to the Web version of this article.)

HD-TDCS montages were inversely proportional, as suggested previously [43]. The interindividual variability of focality was found to be high. For conventional montages, the variability increased as the stimulating electrode size decreased, whereas for both types of HD montages, the variability decreased towards more focal montages.

The interindividual variability in both the predicted EF magnitude and normal component was found to be high at the target point, increasing with smaller stimulating electrodes of the conventional montage. 4×1 HD montages showed a similar pattern, with more focal EFs having higher variability. These results suggest that the increase in EF focality comes at the cost of additional interindividual variability in the EFs. To the best of our knowledge, differences in the variability of different TDCS montages have not been examined in experimental studies. However, Bastani and Jaberzadeh [19] reported higher variability in the after-effects of TDCS with 12 cm^2 electrodes versus 24 cm^2 electrodes. Also, a systematic review by Horvath et al. [47] revealed a higher standard deviation of motor evoked potential amplitudes for high current density montages than for low current density montages. Assuming that differences in current density arise from differently sized anodes, both of these results are in line with the current findings for predicted EFs via computational models.

Importantly, with stimulating electrodes larger than $\text{Ø}3 \text{ cm}$, there are high EFs between the two electrodes, and the maximum EFs lie outside the targeted area. The bipolar HD montages, ML and PA, exploit this phenomenon by targeting the stimulation between the electrodes, and achieve high EFs with a reasonable focality. Importantly, the EF magnitude at the target site for the PA and ML montages had lower interindividual variability than that of the conventional montage with a stimulating electrode size of $7 \times 5 \text{ cm}^2$, while having comparable magnitudes to 4×1 HD-TDCS.

These bipolar HD montages produce approximately perpendicular EF directions at the target compared with other montages (Supplementary figure S2). Additionally, bipolar HD montages benefit from the ability to control the direction of current flow in the brain in relation to the gyri and sulci, which is reported to affect the physiological [14] and behavioral [16] outcomes of TDCS: PA, but not ML or AP (opposite polarity to PA), direction EFs have been found to affect TMS motor evoked potentials [14], and AP, but not PA, direction EFs have been suggested to impair the retention of learning in a ballistic movement task [16]. The lack of control of the direction of the EFs is a potential factor for inter-individual variability in TDCS [16]. Hence, bipolar HD montages are promising for reducing interindividual variability in TDCS EFs, since they have both moderate inter-individual EF variability and the possibility of

controlling EF direction. However, the orientation of this type of montage was found to slightly affect the EF magnitude, focality, and interindividual variability, and the effect of anatomical differences was affected by EF direction. In addition, with studies involving TMS motor evoked potentials, TMS direction was found to affect the outcome of bipolar HD TDCS [14].

For conventional montages, the effect of individual anatomy on the TDCS EFs was found to be affected by the stimulating electrode size, with smaller electrodes showing slightly higher correlation coefficients between the EF magnitude and thicknesses of the scalp, skull, and CSF. For 4×1 HD-TDCS, the effect of skull and skin on the individual EF magnitudes was found to increase with decreasing distance from anode to cathodes. This suggests that focal EFs are more strongly affected by individual anatomy compared with those that are diffuse.

It should be noted that we studied only the EFs on the right hemisphere as the study focused on EFs in the vicinity of the targeted right M1. Compared with HD montages that restrict the current flow between the anode and cathode(s), conventional TDCS also produces EFs on the opposite hemisphere, which could lead to differences in the outcome of stimulation using these methods [17]. In addition, EFs with conventional montages with large stimulating electrodes are highly diffuse, and maximum EFs are located far from the targeted regions [8], which could lead to modulation of different populations of neurons [48] and contribute to inter-individual variability in stimulation outcomes. Previous research has suggested that motor cortex excitability alterations differ between conventional and 4×1 HD TDCS [49]. However, possible differences in the interindividual variability of stimulation outcomes between the two different montage types have not yet been addressed in depth.

The EFs identified in the current study were of the same order of magnitude as those obtained in previous computational studies [8,43,50,51], with variation in the precise magnitudes likely arising from differing conductivity values. For example, the conductivity of the skin in the current study was lower than that used in a previous study [43], resulting in higher EFs. However, skin conductivity may change even during TDCS, since it increased over time as the saline of the electrodes soaked into the skin [52]. Although these modeled EFs tended to be higher than those measured in vivo [20,53,54], the spatial distribution has been found to be highly correlated between the two [20]. The difference in EF magnitude between square and round electrodes with identical surface areas was found to be less than 6% (Supplementary figure S3). Hence, the results can be assumed to be valid for both round and rectangular electrodes. An additional limitation regarding these montages is the electrodes,

which are modeled in all montages as saline soaked sponge electrodes that are commonly used with large rubber electrodes. However, with small electrodes used in HD-TDCS, conductive electrode paste is used instead of saline-soaked sponges [55]. As both saline and electrode paste have similar electrical conductivities (here: 1.6 S/m for saline, Rawji et al. [14]: 1.4 S/m for electrode paste), our results are also valid for paste-type electrodes.

Finally, as we examined EF magnitude, the results are valid for both anodal and cathodal TDCS. The main results are also valid for different stimulating electrode locations, based on the modeling of different stimulating electrode locations (Supplementary figure S4).

Conclusions

We found that the increase in the focality of cortical EFs came at the cost of increasing interindividual variability when conventional (M1–contralateral forehead) and 4×1 HD-TDCS montages were used. Our findings suggest that computational modeling can be used to equalize the EFs of subjects whenever highly focal TDCS montages are used to minimize interindividual variability in EFs. In addition, bipolar HD montages produced relatively focal EFs, as strong as those produced with 4×1 HD-TDCS, but exhibited lower variability than either 4×1 HD or conventional montages.

Funding

The work was supported by grants from the Grants-in-Aid for Scientific Research (JSPS KAKENHI 16H03201 and 17H00869).

Declaration of competing interest

None.

Appendix A. Supplementary data

Supplementary data to this article can be found online at <https://doi.org/10.1016/j.brs.2019.09.017>.

References

- [1] Mutz J, Edgcombe DR, Brunoni AR, Fu CHY. Efficacy and acceptability of non-invasive brain stimulation for the treatment of adult unipolar and bipolar depression: a systematic review and meta-analysis of randomised sham-controlled trials. *Neurosci Biobehav Rev* 2018;92:291–303. <https://doi.org/10.1016/j.neubiorev.2018.05.015>.
- [2] O'Connell NE, Marston L, Spencer S, DeSouza LH, Wand BM. Non-invasive brain stimulation techniques for chronic pain. *Cochrane Database Syst Rev* 2018;(3).
- [3] Fujimoto S, Kon N, Otaka Y, Yamaguchi T, Nakayama T, Kondo K, et al. Transcranial direct current stimulation over the primary and secondary somatosensory cortices transiently improves tactile spatial discrimination in stroke patients. *Front Neurosci* 2016;10:128.
- [4] Hummel F, Celnik P, Giraux P, Floel A, Wu W, Gerloff C, et al. Effects of non-invasive cortical stimulation on skilled motor function in chronic stroke. *Brain* 2005;128:490–9. <https://doi.org/10.1093/brain/awh369>.
- [5] Tanaka S, Takeda K, Otaka Y, Kita K, Osu R, Honda M, et al. Single session of transcranial direct current stimulation transiently increases knee extensor force in patients with hemiparetic stroke. *Neurorehabilitation Neural Repair* 2011;25:565–9.
- [6] Nitsche MA, Cohen LG, Wassermann EM, Priori A, Lang N, Antal A, et al. Transcranial direct current stimulation: state of the art 2008. *Brain Stimul* 2008;1:206–23. <https://doi.org/10.1016/j.brs.2008.06.004>.
- [7] Mikkonen M, Laakso I. Effects of posture on electric fields of non-invasive brain stimulation. *Phys Med Biol* 2019;64:065019.
- [8] Datta A, Bansal V, Diaz J, Patel J, Reato D, Bikson M. Gyri-precise head model of transcranial direct current stimulation: improved spatial focality using a ring electrode versus conventional rectangular pad. *Brain Stimul* 2009;2(20):207. <https://doi.org/10.1016/j.brs.2009.03.005>. e1.
- [9] Wiethoff S, Hamada M, Rothwell JC. Variability in response to transcranial direct current stimulation of the motor cortex. *Brain Stimul* 2014;7:468–75. <https://doi.org/10.1016/j.brs.2014.02.003>.
- [10] López-Alonso V, Cheeran B, Río-Rodríguez D, Fernández-del-Olmo M. Inter-individual variability in response to non-invasive brain stimulation paradigms. *Brain Stimul* 2014;7:372–80. <https://doi.org/10.1016/j.brs.2014.02.004>.
- [11] Laakso I, Tanaka S, Koyama S, De Santis V, Hirata A. Inter-subject variability in electric fields of motor cortical tDCS. *Brain Stimul* 2015;8:906–13. <https://doi.org/10.1016/j.brs.2015.05.002>.
- [12] Opitz A, Paulus W, Will S, Antunes A, Thielscher A. Determinants of the electric field during transcranial direct current stimulation. *Neuroimage* 2015;109:140–50. <https://doi.org/10.1016/j.neuroimage.2015.01.033>.
- [13] Laakso I, Mikkonen M, Koyama S, Hirata A, Tanaka S. Can electric fields explain inter-individual variability in transcranial direct current stimulation of the motor cortex? *Sci Rep* 2019;9:626.
- [14] Rawji V, Ciocca M, Zacharia A, Soares D, Truong D, Bikson M, et al. tDCS changes in motor excitability are specific to orientation of current flow. *Brain Stimul* 2018;11:289–98. <https://doi.org/10.1016/j.brs.2017.11.001>.
- [15] Antonenko D, Thielscher A, Saturnino GB, Aydin S, Iltermann B, Grittmner U, et al. Towards precise brain stimulation: is electric field simulation related to neuromodulation? *Brain Stimul* 2019. <https://doi.org/10.1016/j.brs.2019.03.072>.
- [16] Hannah R, Iacovou A, Rothwell JC. Direction of TDCS current flow in human sensorimotor cortex influences behavioural learning. *Brain Stimul* 2019;12:684–92. <https://doi.org/10.1016/j.brs.2019.01.016>.
- [17] Nitsche MA, Doemkes S, Karaköse T, Antal A, Liebetanz D, Lang N, et al. Shaping the effects of transcranial direct current stimulation of the human motor cortex. *J Neurophysiol* 2007;97:3109–17.
- [18] Faria P, Hallett M, Miranda PC. A finite element analysis of the effect of electrode area and inter-electrode distance on the spatial distribution of the current density in tDCS. *J Neural Eng* 2011;8:066017.
- [19] Bastani A, Jaberzadeh S. A-tDCS differential modulation of corticospinal excitability: the effects of electrode size. *Brain Stimul* 2013;6:932–7. <https://doi.org/10.1016/j.brs.2013.04.005>.
- [20] Opitz A, Yeagle E, Thielscher A, Schroeder C, Mehta AD, Milham MP. On the importance of precise electrode placement for targeted transcranial electric stimulation. *Neuroimage* 2018;181:560–7. <https://doi.org/10.1016/j.neuroimage.2018.07.027>.
- [21] Bortoletto M, Rodella C, Salvador R, Miranda PC, Miniussi C. Reduced current spread by concentric electrodes in transcranial electrical stimulation (tES). *Brain Stimul* 2016;9:525–8. <https://doi.org/10.1016/j.brs.2016.03.001>.
- [22] Fischer DB, Fried PJ, Ruffini G, Ripolles O, Salvador R, Banus J, et al. Multifocal tDCS targeting the resting state motor network increases cortical excitability beyond traditional tDCS targeting unilateral motor cortex. *Neuroimage* 2017;157:34–44. <https://doi.org/10.1016/j.neuroimage.2017.05.060>.
- [23] Mikkonen M, Laakso I, Sumiya M, Koyama S, Hirata A, Tanaka S. TMS motor thresholds correlate with TDCS electric field strengths in hand motor area. *Front Neurosci* 2018;12:426.
- [24] Laakso I, Tanaka S, Mikkonen M, Koyama S, Sadato N, Hirata A. Electric fields of motor and frontal tDCS in a standard brain space: a computer simulation study. *Neuroimage* 2016;137:140–51. <https://doi.org/10.1016/j.neuroimage.2016.05.032>.
- [25] Dale AM, Fischl B, Sereno MI. Cortical surface-based analysis: I. Segmentation and surface reconstruction. *Neuroimage* 1999;9:179–94. <https://doi.org/10.1006/nimg.1998.0395>.
- [26] Fischl B, Sereno MI, Dale AM. Cortical surface-based analysis: II: inflation, flattening, and a surface-based coordinate system. *Neuroimage* 1999;9:195–207. <https://doi.org/10.1006/nimg.1998.0396>.
- [27] Fischl B, Dale AM. Measuring the thickness of the human cerebral cortex from magnetic resonance images. *Proc Natl Acad Sci USA* 2000;97:11050–5.
- [28] Desikan RS, Ségonne F, Fischl B, Quinn BT, Dickerson BC, Blacker D, et al. An automated labeling system for subdividing the human cerebral cortex on MRI scans into gyral based regions of interest. *Neuroimage* 2006;31:968–80. <https://doi.org/10.1016/j.neuroimage.2006.01.021>.
- [29] Freygang Jr WH, Landau WM. Some relations between resistivity and electrical activity in the cerebral cortex of the cat. *J Cell Comp Physiol* 1955;45:377–92.
- [30] Stoy RD, Foster KR, Schwan HP. Dielectric properties of mammalian tissues from 0.1 to 100 MHz; a summary of recent data. *Phys Med Biol* 1982;27:501–13.
- [31] Gabriel C, Gabriel S, Corthout E. The dielectric properties of biological tissues: I. Literature survey. *Phys Med Biol* 1996;41:2231–49.
- [32] Ranck JB. Specific impedance of rabbit cerebral cortex. *Exp Neurol* 1963;7:144–52. [https://doi.org/10.1016/S0014-4886\(63\)80005-9](https://doi.org/10.1016/S0014-4886(63)80005-9).
- [33] Latiikka J, Kuurne T, Eskola H. Conductivity of living intracranial tissues. *Phys Med Biol* 2001;46:1611–6.
- [34] Akhtari M, Salamon N, Duncan R, Fried I, Mathern GW. Electrical conductivities of the freshly excised cerebral cortex in epilepsy surgery patients; correlation with pathology, seizure duration, and diffusion tensor imaging. *Brain Topogr* 2006;18:281.
- [35] Baumann SB, Wozny DR, Kelly SK, Meno FM. The electrical conductivity of human cerebrospinal fluid at body temperature. *IEEE (Inst Electr Electron Eng) Trans Biomed Eng* 1997;44:220–3.
- [36] Akhtari M, Bryant HC, Mamelak AN, Flynn ER, Heller L, Shih JJ, et al. Conductivities of three-layer live human skull. *Brain Topogr* 2002;14:151–67.
- [37] Gabriel C, Peyman A, Grant EH. Electrical conductivity of tissue at frequencies below 1 MHz. *Phys Med Biol* 2009;54:4863–78.
- [38] Lindenblatt G, Silny J. A model of the electrical volume conductor in the region of the eye in the ELF range. *Phys Med Biol* 2001;46:3051–9.

- [39] Laakso I, Hirata A. Fast multigrid-based computation of the induced electric field for transcranial magnetic stimulation. *Phys Med Biol* 2012;57:7753–65.
- [40] Soldati M, Mikkonen M, Laakso I, Murakami T, Ugawa Y, Hirata A. A multi-scale computational approach based on TMS experiments for the assessment of electro-stimulation thresholds of the brain at intermediate frequencies. *Phys Med Biol* 2018;63:225006.
- [41] Fonov VS, Evans AC, McKinstry RC, Almlí CR, Collins DL. Unbiased nonlinear average age-appropriate brain templates from birth to adulthood. *Neuroimage* 2009;47:S102.
- [42] Fonov V, Evans AC, Botteron K, Almlí CR, McKinstry RC, Collins DL. Unbiased average age-appropriate atlases for pediatric studies. *Neuroimage* 2011;54:313–27. <https://doi.org/10.1016/j.neuroimage.2010.07.033>.
- [43] Alam M, Truong DQ, Khadka N, Bikson M. Spatial and polarity precision of concentric high-definition transcranial direct current stimulation (HD-tDCS). *Phys Med Biol* 2016;61:4506–21.
- [44] Borckardt JJ, Bikson M, Frohman H, Reeves ST, Datta A, Bansal V, et al. A pilot study of the tolerability and effects of high-definition transcranial direct current stimulation (HD-tDCS) on pain perception. *J Pain* 2012;13:112–20. <https://doi.org/10.1016/j.jpain.2011.07.001>.
- [45] Spampinato DA, Satar Z, Rothwell JC. Combining reward and M1 transcranial direct current stimulation enhances the retention of newly learnt sensorimotor mappings. *Brain Stimul* 2019. <https://doi.org/10.1016/j.brs.2019.05.015>.
- [46] Çan MK, Laakso I, Nieminen JO, Murakami T, Ugawa Y. Coil model comparison for cerebellar transcranial magnetic stimulation. *Biomed Phys Eng Express* 2018;5:015020.
- [47] Horvath JC, Forte JD, Carter O. Evidence that transcranial direct current stimulation (tDCS) generates little-to-no reliable neurophysiologic effect beyond MEP amplitude modulation in healthy human subjects: a systematic review. *Neuropsychologia* 2015;66:213–36. <https://doi.org/10.1016/j.neuropsychologia.2014.11.021>.
- [48] Radman T, Ramos RL, Brumberg JC, Bikson M. Role of cortical cell type and morphology in subthreshold and suprathreshold uniform electric field stimulation in vitro. *Brain Stimul* 2009;2(21). <https://doi.org/10.1016/j.brs.2009.03.007>. 228.e3.
- [49] Kuo H, Bikson M, Datta A, Minhas P, Paulus W, Kuo M, et al. Comparing cortical plasticity induced by conventional and high-definition 4×1 ring tDCS: a neurophysiological study. *Brain Stimul* 2013;6:644–8. <https://doi.org/10.1016/j.brs.2012.09.010>.
- [50] Datta A. Inter-individual variation during transcranial direct current stimulation and normalization of dose using MRI-derived computational models. *Front Psychiatry* 2012;3:91.
- [51] Bai S, Dokos S, Ho K, Loo C. A computational modelling study of transcranial direct current stimulation montages used in depression. *Neuroimage* 2014;87:332–44. <https://doi.org/10.1016/j.neuroimage.2013.11.015>.
- [52] Gomez-Tames J, Sugiyama Y, Laakso I, Tanaka S, Koyama S, Sadato N, et al. Effect of microscopic modeling of skin in electrical and thermal analysis of transcranial direct current stimulation. *Phys Med Biol* 2016;61:8825–38.
- [53] Opitz A, Falchier A, Yan C, Yeagle EM, Linn GS, Megevand P, et al. Spatio-temporal structure of intracranial electric fields induced by transcranial electric stimulation in humans and nonhuman primates. *Sci Rep* 2016;6:31236.
- [54] Huang Y, Liu AA, Lafon B, Friedman D, Dayan M, Wang X, et al. Measurements and models of electric fields in the in vivo human brain during transcranial electric stimulation. *eLife* 2017;6:e18834.
- [55] Villamar MF, Volz M, Sarah, Bikson M, Datta A, DaSilva AF, Fregni F. Technique and considerations in the use of 4×1 ring high-definition transcranial direct current stimulation (HD-tDCS). *J Vis Exp* 2013:e50309.